ADVANCED OPTICAL MATERIALS
www.advopticalmat.de

Wet Chemical Engineering of Nanostructured GRIN Lenses

I. Brian Becerril-Castro, Mariacristina Turino, Nicolas Pazos-Perez, Xiao Xiaofei, Tadzio Levato, Stefan A. Maier, Ramon A. Alvarez-Puebla,* and Vincenzo Giannini**

Gradient-index (GRIN) lenses have long been recognized for their importance in optics as a result of their ability to manipulate light. However, traditional GRIN lenses are limited on a scale of tens of microns, impeding their integration into nanoscale optical devices. This study presents a groundbreaking self-assembled method that overcomes this limitation, allowing for constructing GRIN lenses at an extremely small dimension. The self-assembly process offers several advantages, including creating highly precise, scalable, cost-effective, and complex structures that eliminate the need for intricate and time-consuming manual assembly. By engineering densely packed arrays of metallic nanoparticles, exceptional control over the local refractive index has been achieved. This is accomplished by layer-by-layer assembly of gold nanoparticles of different sizes over silica beads. A GRIN lens light-sink is built where light is preferentially directed toward the center, which is corroborated by measuring the fluorescence of Rhodamine B (RhB) in the inside. Unlike traditional bulky macroscopic GRIN lenses, light-sinks boast a size under 2.5 µm. Notably, the self-focusing effects of this design allowed us to track the growth of single-nanoparticle layers using SERS (Surface-Enhanced Raman Spectroscopy). These results pave the way for designing and developing lens-like devices at the nanoscale, allowing unprecedented light manipulation.

1. Introduction

Recent developments in metamaterials have demonstrated that compact metallic metamaterials can provide highly transparent metallic structures with engineerable refractive indexes for all wavelengths within or beyond the near-infrared;[1,2] moreover, high refractive indexes are possible in the visible region.[3] In addition to being transparent, such metamaterials also provide extremely strong electromagnetic field enhancements in the gaps between metal nanoparticles (hot-spots), making them attractive as engineered surface-enhanced Raman scattering (SERS) substrates.[4,5] Due to their unique properties, we refer to these metamaterials as transparent metals to highlight their effective dielectric character even if made of metallic components. These structures allow for materials to be designed with a desired refractive index profile. The ability to change the refractive index locally is critical for high-performance optical devices. Such devices are also known as gradient index lenses (GRINs),[6] and while they are commonly found as classical bulky structures,[7] there is a high interest in their development at the microscale and their integration into complex systems such as achromatic microlenses[8] or optical fibers used in optofluidic systems.[9] In this work, we show that we can extend GRIN lenses to the field of nano-optics thanks to the layer-by-layer method and the transparent metal idea, opening the exploration of lens-like devices at the nanoscale. As a proof of concept, we design, fabricate, and explore a useful structure in nonlinear optics and spectroscopy (i.e., a spherical metaparticle that focuses light at its

I. B. Becerril-Castro, M. Turino, N. Pazos-Perez, R. A. Alvarez-Puebla
Department of Physical and Inorganic Chemistry
Universitat Rovira i Virgili
43007 Tarragona, Spain
E-mail: ramon.alvarez@urv.cat

X. Xiaofei, T. Levato, V. Giannini
Technology Innovation Institute
P.O. Box 9639, Abu Dhabi United Arab Emirates
E-mail: vincenzo.giannini@tii.ae

The ORCID identification number(s) for the author(s) of this article can be found under https://doi.org/10.1002/adom.202400485

DOI: 10.1002/adom.202400485

S. A. Maier
School of Physics and Astronomy
Monash University
VIC 3800 Clayton, Australia
E-mail: stefan.maier@monash.edu

S. A. Maier
Department of Physics
Imperial College London
London SW7 2AZ, UK

R. A. Alvarez-Puebla
Institució Catalana de Recerca i Estudis Avançats
08010 Barcelona, Spain

V. Giannini
Instituto de Estructura de la Materia, CSIC
610101 Madrid, Spain

V. Giannini
Centre of Excellence ENSEMBLE3 sp. z o.o.
01-919 Warsaw, Poland

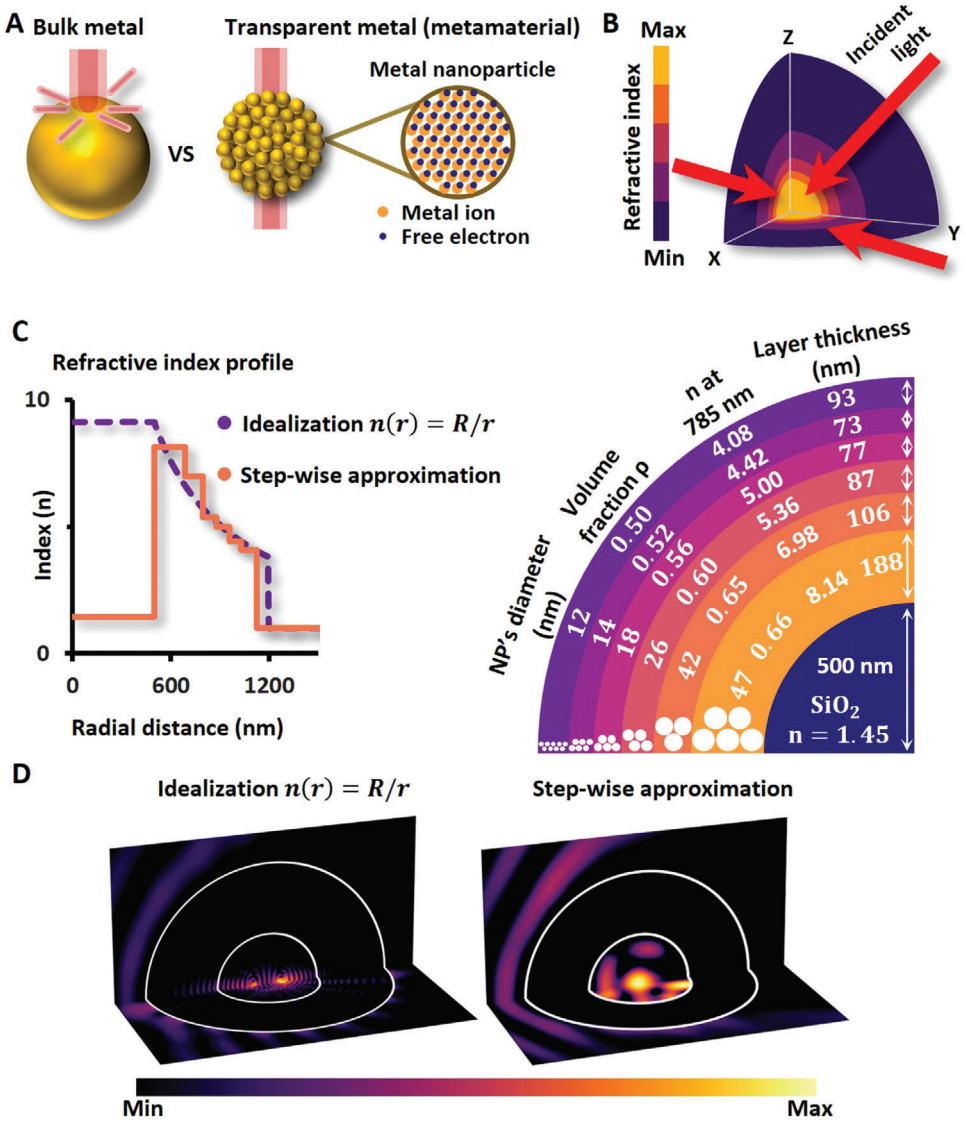

Figure 1. Effective medium approximation for a transparent metal. A) Comparison of the behavior between a bulk metal and a transparent metal. B) The light impinging on a light-sink particle C) Refractive index profile for an ideal and an experimental light-sink, dotted, and solid lines, respectively. D) Simulation of the electric field intensity for both refractive index profiles with an excitation plane wave at 785 *nm*.

center, which effectively will act as a light sink). Remarkably, the engineered GRIN lens exhibits the desired behavior within, but not limited to, sizes less than 2.5 μ m, and since multiple lenses are produced during fabrication, this procedure can be mass scalable. These results show the versatility of creating desired transparent metamaterials with unprecedented control of the local refractive index.

2. Results and Discussion

The different optical behavior of a metastructure composed of close-packed metal nanoparticles (NPs) and a bulk gold metallic particle with the same dimension and shape in the near-infrared region and lower energy is illustrated in **Figure** 1A. Due to the small dimensions of the constituting NPs compared with the incident wavelength, the nanostructured metamaterial can behave as an effective dielectric medium.[1,2] Thus, being a transparent material in contrast to the highly reflective behavior provided by the bulk metal. This counterintuitive behavior is due to the limitation of the conduction electrons' ability to travel and oscillate only inside the NPs and behave like an atom in a dielectric. Of course, to confine the electron movement, each NP must be isolated with an insulating layer. The effective refractive index of such a structure can be obtained numerically, solving the complex band structure of the considered system using the eigenvalue equation:

$$\Theta(\mathbf{k})\mathbf{u}(\mathbf{k}) = \omega^2(\mathbf{k})\mathbf{u}(\mathbf{k}) \quad (1)$$

where k is the wave-vector, $\mathbf{u}$ is the electric or magnetic field and Θ is the corresponding eigenoperator.[1]

Traditionally, the band calculation is done by solving the eigenvalue problem that links the frequency ω with the permittivity ϵ

and permeability μ at any particular position in the Brillouin zone with k-vector **k**:

$$\omega = \omega\left(\varepsilon(\omega), \mu(\omega), k_x, k_y, k_z\right) \tag{2}$$

However, it turns out that instead of solving for frequency, in this case (highly conducting metals), it is more convenient if we solve directly for the Bloch wave vector,[1]

$$k_z = k_z\left(\varepsilon(\omega), \mu(\omega), k_x, k_y, \omega\right) \tag{3}$$

where we choose k_z as the propagation direction.[1] In this way, we solve for the effective index of compact metallic structures with high accuracy, using finite-differences or finite-elements to discretize our system. Interestingly, when the particles are much smaller than the wavelength, even in the case of small gaps (when multipolar orders are expected), the following simple Maxwell-Garnett approximation gives accurate results:[2]

$$\epsilon_{eff} = \epsilon_m \frac{2\rho(\epsilon_i - \epsilon_m) + \epsilon_i + 2\epsilon_m}{2\epsilon_m + \epsilon_i - \rho(\epsilon_i - \epsilon_m)} \tag{4}$$

where, ϵ_{eff} is the effective dielectric constant of the medium, ϵ_i of the inclusions, and ϵ_m of the matrix; and ρ is the volume fraction of the inclusions. The above expression considers spherical inclusions. However, it can be shown that we can obtain analytical expressions for the effective refractive index when metal nanoparticles have simple shapes such as cubes, cylinders, etc.[2]

A spherical optical "light concentrator," that is, a structure that focuses light at its center[2] Theoretically, this is obtained in a spherical structure with radius R where the refractive index goes from 1, on the surface, to infinity at the center of the structure (see Figure 1B) in the following way: $n(r) = R/r$, where r is the distance from the center.[2] Such a system does not exist in practice because the refractive index diverges at the center. However, We can create an approximated light concentrator by restricting the effective index, e.g., $1 < n < 9$. This restriction in the refractive index is depicted as a dotted line in Figure 1C. By doing so, we show in Figure 1D that the impinging plane wave (785 nm, $R = 4560$ nm) is focused inside the structure (electric near-field intensity obtained using a recursive transfer-matrix method implemented in the STRATIFY package).[10]

To approximate the light-sink structure with a more realistic design, we approximate the ideal refractive index with a stepwise function shown as a continuous line in Figure 1C. Therefore, we selected and subsequently synthesized six citrate-stabilized gold nanoparticles (AuNPs) of different sizes that matched the proposed refractive profile, following the procedures in the literature.[11] The respective values for the refractive index were calculated using the Maxwell-Garnet approximation (Equation 4) for a wavelength of 785 nm and using the experimental values of evaporated gold for the dielectric constant.[12]

We consider the MUA-BT and the PEI between particles as a net separation of 2 nm. For the volume fraction, an ideal face center cubic packing for the NPs ($\rho = 0.74$) was used. Thus, the refractive index was estimated as 4.08, 4.42, 5.00, 5.36, 6.98, and 8.14 from the outside to the inside layer. These NPs serve as building blocks to create the gradient index on the material since we can control the refractive index with the size and separation of the constituent NPs, producing higher refractive indexes than conventional materials.[13] Other related parameters of the design, such as the NP diameter and the layer thickness, are depicted in Figure 1C. We repeat the simulation for the near-field enhancement using the proposed step-wise refractive index profile. The resulting distribution of the electric field also focuses the light inside the structure, as shown in Figure 1D, despite obvious limitations with the step-wise approximation. The major difference arises from the relatively small index in the interior of the experimental lens. Such a small index in the interior is given by the limitation in the available materials with a high refractive index and a size that we can easily monitor using optical microscopy.

Figure 2A shows representative TEM images of the 47 ± 2, 42 ± 5, 26 ± 3, 18 ± 2, 14 ± 2, and 12 ± 2nm diameter AuNPs, as well as corresponding histograms and higher magnification images of each particle size as insets. The narrow distribution obtained was the first feature that we identify as a priority for producing the light-sink. Figure 2B confirms that the experimental surface plasmon resonances are in between 518 and 533 nm, with a redshift directly related to the increase in size according to the Mie Theory.[14] After the synthesis and characterization, the AuNPs were first functionalized with mercaptoundecanoic acid (MUA) and then with benzenethiol (BT) to obtain Au@MUA-BT NPs. This two-step procedure (Figure 2C) removes the citrate anions from the NPs' surface and mitigates the NPs' aggregation upon the addition of the BT while preserving the negative charge at the surface of the NPs.[15] Also, this electrostatically stabilized colloid yields a strong SERS signal upon excitation with light due to the unsaturated ring of the BT, while the MUA is optically inert (for SERS purposes).[16] The resulting SERS spectra of the functionalized NPs were recorded in suspension using a 785 nm laser and presented in Figure 2D. It can be observed that the intensity of the signal increases rapidly with the increase in the size of the NPs, which is attributed to the increase in the local field enhancement in the proximity of the surface. The characteristic vibrational features of this molecular probe (BT) include the bands centered at 685 cm^{-1} (ring in-plane deformation), 995 cm^{-1} (CH in-plane deformation), 1022 and 1074 cm^{-1} (CC ring breathing).[17]

After preparing the Au@MUA-BT NPs, a SiO_2 bead of 1 μm was selected to serve as a primary scaffold for the multiple layers of NPs that integrate the spherical GRIN lens. We employed the layer-by-layer (LBL) self-assembly paradigm to obtain uniform layers. **Figure 3A** illustrate a description of the assembly method. First, the SiO_2 core (ζ-potential =−55 mV) was coated with sequential layers of polyelectrolytes: initially a positively charged branched polyethyleneimine (PEI); then a negatively charged poly(acrylic acid), PAA; and finally another layer of PEI (final ζ-potential =+53 mV). Then an excess of the previously prepared Au47@MUA-BT NPs was combined with the coated silica to produce hybrid plasmonic microparticles (ζ-potential =−35 mV) via electrostatic adhesion. In Figure 3B, we can see a uniform coating on the surface for the first layer. To continue lens assembly, a further PEI coating was carried out on the so-formed microparticles to reverse surface charge (+40 mV), followed by the mixture with another excess of Au47@MUA-BT NPs. This iterative process was repeated to obtain 5, 3, 4, 5, 6, and 9 layers of functionalized NPs of 47, 42, 26, 18, 14, and 12 nm diameters, in this order.

TEM images of each layer are shown in Figure 3B and Figure S1 (Supporting Information). As the assembly increases

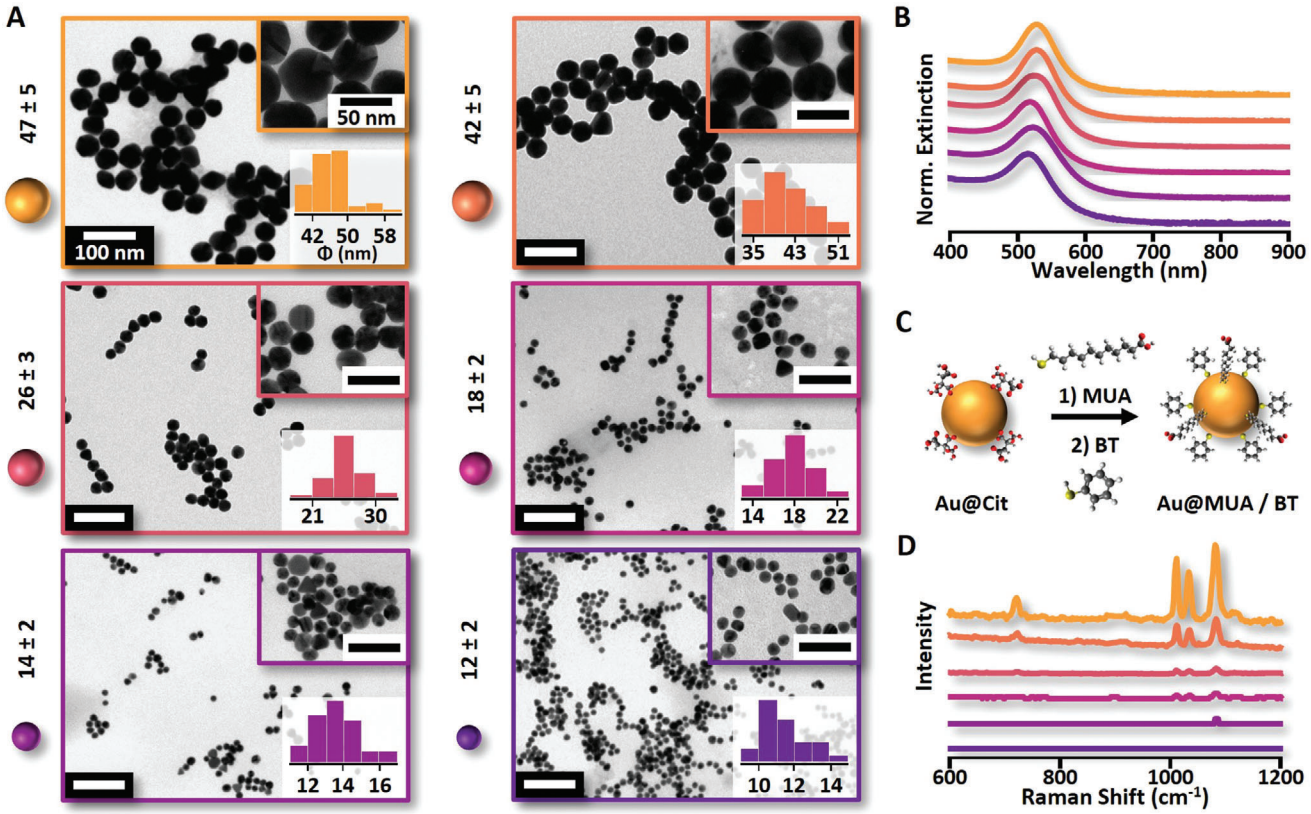

Figure 2. Summary of the AuNPs employed as building blocks for the light-sink. A) Representative TEM images of the AuNPs. Corresponding higher magnification images and histograms are presented as insets. B) UV–vis spectra of the corresponding AuNPs are shown in (A). C) Schematic representation of the functionalization with mercaptoundecanoic acid (MUA) and benzenethiol (BT) of the citrate stabilized AuNPs. D) SERS spectra of the BT functionalized AuNPs using a 785 *nm* laser.

its complexity, the hybrid beads acquire an asymmetric morphology (compare from the 6th to 14th layers with the first layer); however, this behavior is reversed into a more regular shape as more layers are integrated (see last five layers). The LBL method employed relays in the electrostatic attraction between the last layer (positively charged because of the PEI wrapping) and the functionalized Au@MUA-BT NPs (negatively charged). Therefore, the ζ-potential values were monitored after each step (Figure 3C) to ensure the change in charge and the adherence of the new layer of NPs. Additionally, the mixture of polyelectrolytes and MUA with BT on both sides of the NPs prevents direct contact among the metallic NPs, effectively isolating the NPs and, therefore, stopping the electrons from traveling from one NP to a neighbor. Another point to recall is that even when we use a 1µ *m* SiO_2 bead as a core, it is possible to use smaller beads if necessary.

A first optical characterization of the lens was performed using a 785 nm laser line as the excitation source. The characterization was carried out by spin-coating the individual beads on a glass and acquiring the SERS spectra. The average intensity of the peak at 1070 cm^{-1} of each layer is represented in **Figure** 4A, as well as the full SERS spectra of the BT on the GRIN lens (as inset). The growing steps of the lens are divided into six sets according to the size of the NPs (separated by color), and on each, a decreasing tendency is observed with the increasing number of layers. These results may appear contradictory with the literature since the formation of NPs assembles promotes an exponential increase of the SERS signal compared with isolated NP.[18] However, these apparently contradictory results can be explained using the transparent metal idea: compact metallic metamaterials can behave as transparent metallic structures with engineerable refractive indexes. In particular, films of closed-packaged AuNPs of 60,[1] 33,[19] and 15[20] nm in diameter have been previously reported (theoretically and experimentally) with a high transmittance in the NIR region, and with engineerable losses on the visible region depending on the configuration of the system and the polarization of the light. Thus, we can expect that in our spherical system, as more layers of equal-sized NPs are assembled over the microbead, the random empty spaces are reduced and occupied by NPs. Hence, the approximation as a dielectric medium on such region becomes more valid and creates a larger effective dielectric area where the light can travel and concentrate towards the inside, decreasing the radiated SERS signal. Therefore, we have a first indication of lens behavior in our system that contrasts with similar structures, such as plasmonic supercrystals.[21]

The final corroboration of the behavior of the lens as a light sink was the measurement of the fluorescence emitted by a dye on the interior of the silica bead. The selected dye was Rhodamine B (RhB), which was previously encapsulated on the interior of

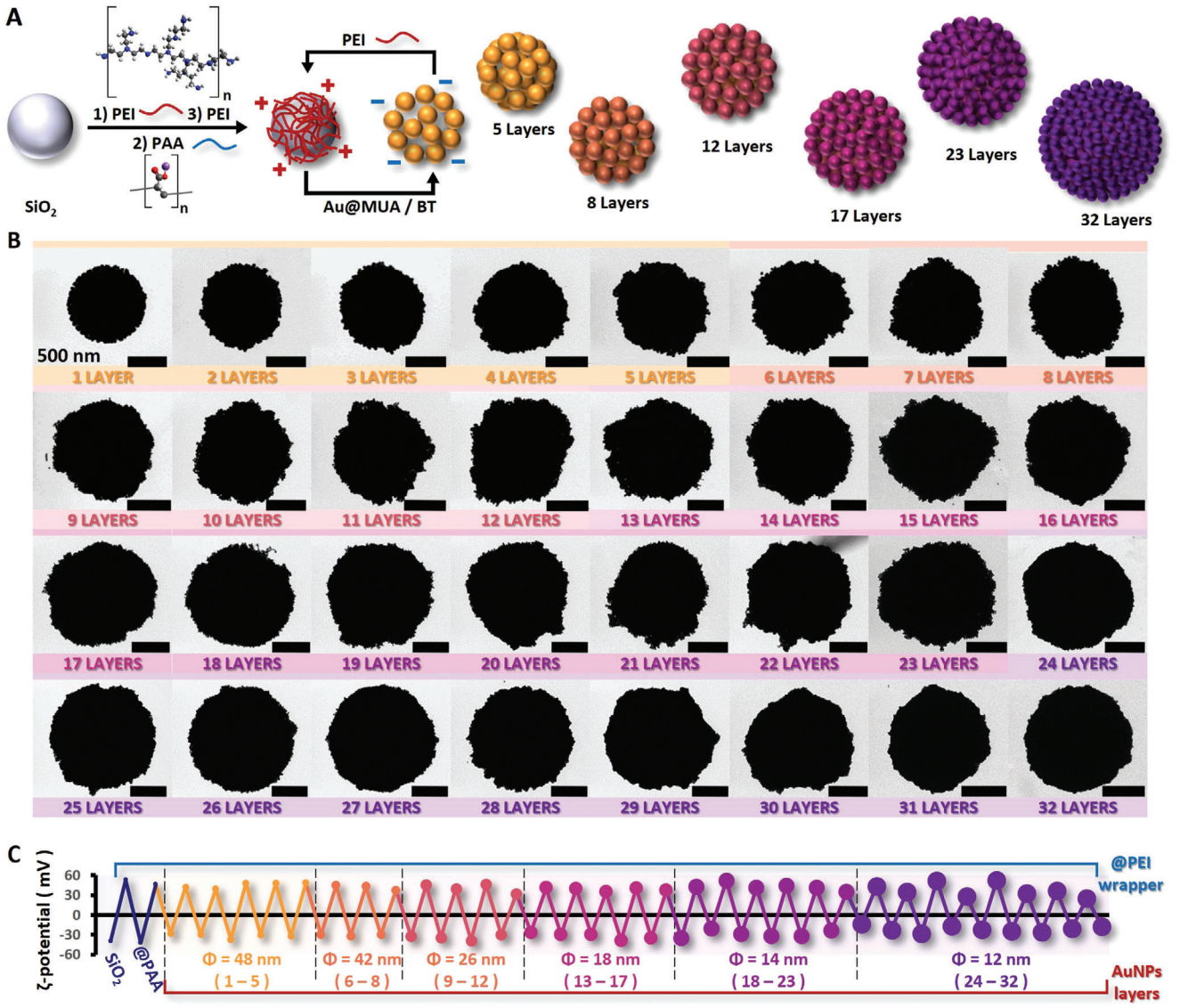

Figure 3. Illustrative description of the assembling approach. A) Schematic of the cyclic procedure using opposite charges. B) Representative TEM images of each of the sequential 32 layers of the assembly. C) $\zeta - potential$ monitoring of the assembly process.

the silica bead that serves as a scaffold for the lens (see Supporting Information). The presence of RhB do not change the previously discussed behavior on the SERS signal (Figure S3, Supporting Information). The measured emission spectra of the lens (with different layers) excited with a 532 nm laser are presented in **Figure** 5A. As inset, a diagram of the idealized phenomenon is displayed, i.e., light is focused on the particle's interior, producing fluorescence. The peak within the 566–570 nm range matches the characteristics of RhB, confirming its presence. Consequently, we infer that light successfully penetrates the interior of the bead. In Figure 5B, we plot the maximum intensity against the number of layers in the lens, where an increase in the fluorescence is clearly noted on a lens with two layers. This abrupt increase suggests that the lens conveys a light concentrator behavior because it more effectively meets the required conditions of the effective media approximation as previously postulated and imposes a minimum of two layers for better performance. Plotting the fluorescence maximum intensity from layers 2 to 5 as an inverse of the distance to the central bead (inset Figure 5B), a lineal trend is observed (R2 = 0.9929); thus, the intensity decreases inversely with the thickness of the lens. These significant losses are attributed to optical absorption because the imaginary part of the calculated effective dielectric constant for 532 nm is bigger than the real ($\epsilon_{eff} = 0.81 + 2.20i$). The numerical simulation considering two layers (inset Figure 5B) also supports that the light initiates focusing toward the center, albeit not completely, is enough to increase the fluorescence experimentally. As previously stated, the SERS signal simultaneously decreases on the change from 1 to 2 layers. Therefore, we must conclude that the evidence points towards the successful development of a light sink: a structure that focuses light in its center.

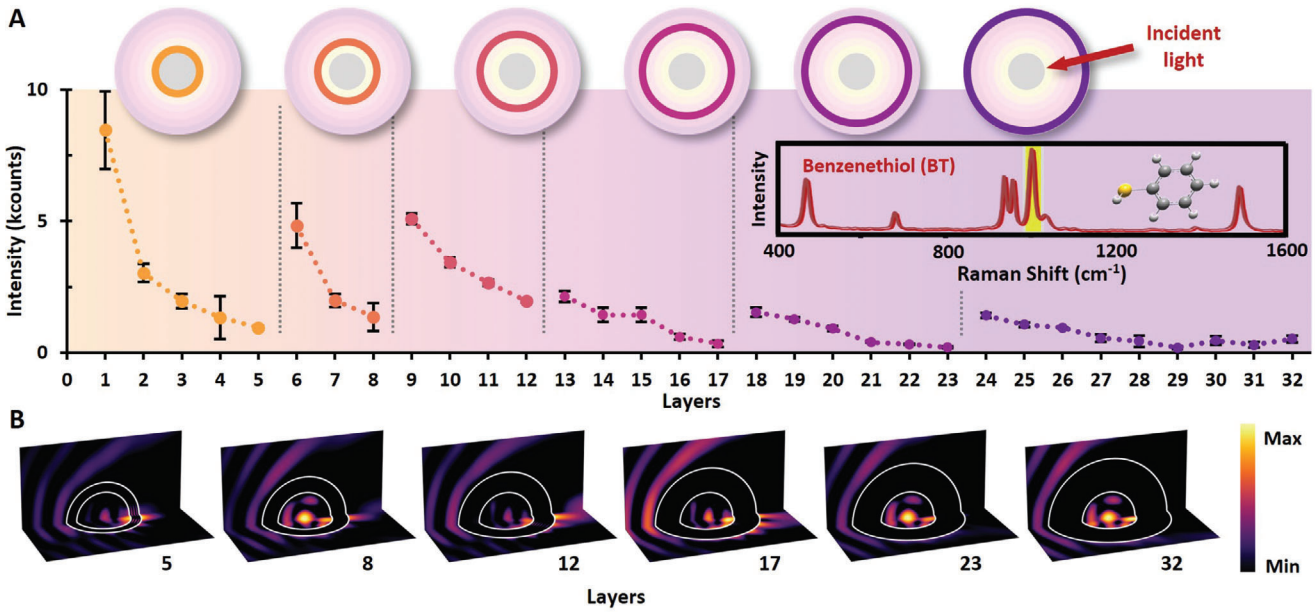

Figure 4. Light sink optical behavior varying the number of layers. A) SERS intensity sink of the 1070 cm^{-1} breathing mode of benzenethiol as a function of the layer number. Extended BT spectrum as inset. B) Near-field simulation at 785 *nm* for a light sink with 5, 8, 12, 17, 23, or 32 layers.

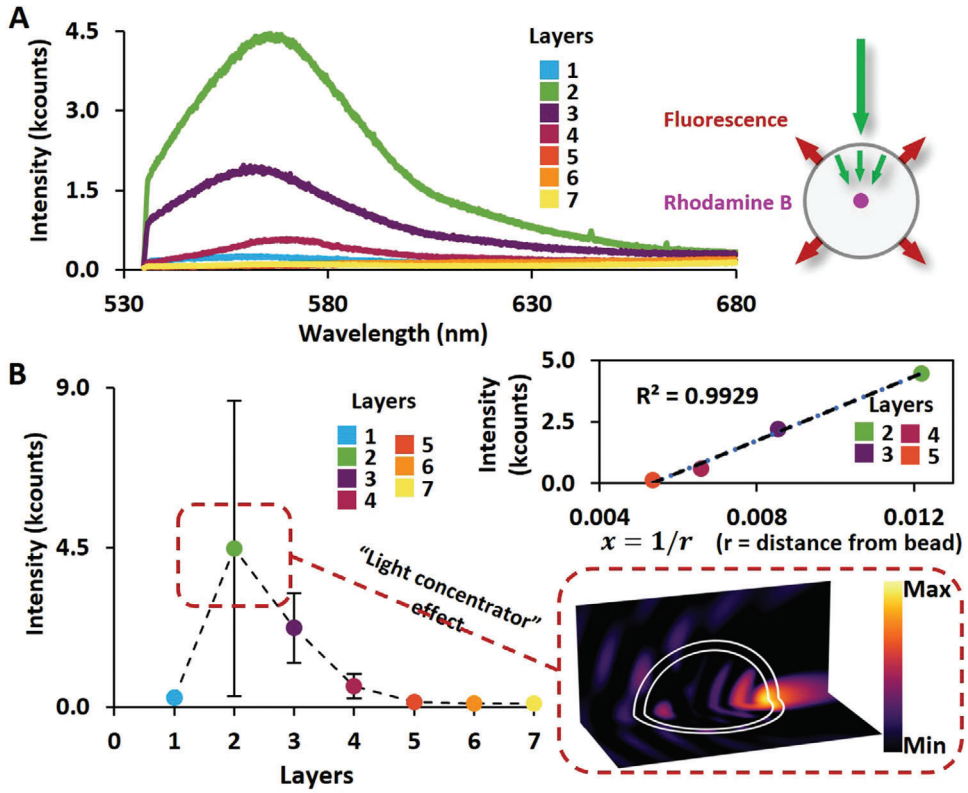

Figure 5. Fluorescence of Rhodamine B in the sink optical. A) Fluorescence spectra as a function of the layer number. Illustrative diagram of the process as inset. B) Fluorescence intensity as a function of the layer number. As inset: linear adjustment for the distance inverse from the bead's surface (layers 2–5) and numerical simulation considering of two layers.

3. Conclusion

We have constructed and characterized optical nanolens with intriguing properties. Specifically, we have developed a GRIN lens that acts as a light sink, focusing light toward its center. Notably, this nanolens is remarkably small, measuring less than 2.5 μm, distinguishing it from conventional bulky GRIN lenses.

What makes such nanolens remarkable is their ability to exhibit self-focusing effects, enabling us to investigate the influence of single nanoparticle layers in a transparent metal, observing deviation from effective media theory when there are changes in particle dimensions. Surprisingly, these effects were noticeable with only two layers of nanoparticles, indicating that precise control over the refractive index can be achieved below the 100 *nm* threshold for near-infrared light.

These findings offer a potential avenue for the design of nanoscale lenses and lens-like devices. By exploring the possibilities of nanoscale lens design, we contribute to advancing this field and opening up new possibilities for future applications.

Supporting Information

Supporting Information is available from the Wiley Online Library or from the author.

Acknowledgements

I.B.B.-C. and M.T. contributed equally to this work. This research was supported by the projects PID2020-120306RB-I00 (funded by MCIN/AEI/10.13039/ 501100011033), PDC2021-121787-I00 (funded by MCIN/AEI/10.13039/501100011033 and European Union Next Generation EU/PRTR), 2020SGR00166 (funded by Generalitat de Cataluña) and 2021PFR-URV-B2-02 (funded by Universitat Rovira i Virgili). This project has received funding from the European Union's Horizon 2020 Research and Innovation Programme under the Marie Skłodowska-Curie grant agreement no. 713679 and from the Universitat Rovira i Virgili. V.G. thanks the "ENSEMBLE 3 – Centre of Excellence for nanophotonics, advanced materials and novel crystal growth-based technologies" Project (GA No. MAB/2020/14) carried out within the International Research Agendas program of the Foundation for Polish Science co-financed by the European Union under the European Regional Development Fund. S.A.M. acknowledged the EPSRC (EP/W017075/1), the ARC (DP220102152), and the Lee-Lucas Chair in Physics.

Conflict of Interest

The authors declare no conflict of interest.

Data Availability Statement

The data that support the findings of this study are available from the corresponding author upon reasonable request.

Keywords

GRIN lens, hierarchical plasmonic nanostructures, nanolenses

Received: February 20, 2024
Revised: March 28, 2024
Published online: April 26, 2024

[1] S. J. Palmer, X. Xiao, N. Pazos-Perez, L. Guerrini, M. A. Correa-Duarte, S. A. Maier, R. V. Craster, R. A. Alvarez-Puebla, V. Giannini, *Nat. Commun.* **2019**, *10*, 1.
[2] X. Xiao, M. Turino, I. B. Becerril-Castro, S. A. Maier, R. A. Alvarez-Puebla, V. Giannini, *Adv. Photonics Res.* **2022**, *3*, 2200190.
[3] Y.-Y. Zhao, Y.-L. Zhang, M.-L. Zheng, X.-Z. Dong, X.-M. Duan, Z.-S. Zhao, *Laser Photonics Rev.* **2016**, *10*, 665.
[4] J. Langer, D. Jimenez De Aberasturi, J. Aizpurua, R. A. Alvarez-Puebla, B. Auguié, J. J. Baumberg, G. C. Bazan, S. E. J. Bell, A. Boisen, A. G. Brolo, J. Choo, D. Cialla-May, V. Deckert, L. Fabris, K. Faulds, F. J. García De Abajo, R. Goodacre, D. Graham, A. J. Haes, C. L. Haynes, C. Huck, T. Itoh, M. Käll, J. Kneipp, N. A. Kotov, H. Kuang, E. C. Le Ru, H. K. Lee, J.-F. Li, X. Y. Ling, et al., *ACS Nano* **2020**, *14*, 28.
[5] S. Schlücker, *Angew. Chem. Int. Ed. Engl.* **2014**, *53*, 4756.
[6] C. Gomez-Reino, M. Perez, C. Bao, M. Flores-Arias, *Laser Photonics Rev.* **2008**, *2*, 203.
[7] D. T. Moore, *Appl. Opt.* **1980**, *19*, 1035.
[8] C. A. Richards, C. R. Ocier, D. Xie, H. Gao, T. Robertson, L. L. Goddard, R. E. Christiansen, D. G. Cahill, P. V. Braun, *Nat. Commun.* **2023**, *14*, 1.
[9] R. Kasztelanic, A. Filipkowski, A. Anuszkiewicz, P. Stafiej, G. Stepniewski, D. Pysz, K. Krzyzak, R. Stepien, M. Klimczak, R. Buczynski, *Sci. Rep.* **2018**, *8*, 1.
[10] I. L. Rasskazov, P. S. Carney, A. Moroz, *OSA Contin.* **2020**, *3*, 2290.
[11] N. Pazos-Perez, J. M. Fitzgerald, V. Giannini, L. Guerrini, R. A. Alvarez-Puebla, *Nanoscale Adv.* **2019**, *1*, 122.
[12] P. B. Johnson, R. W. Christy, *Phys. Rev. B* **1972**, *6*, 4370.
[13] J. Huh, K. Kim, E. Im, J. Lee, Y. Cho, S. Lee, *Adv. Mater.* **2020**, *32*, 2001806.
[14] J. Zhao, A. O. Pinchuk, J. M. Mcmahon, S. Li, L. K. Ausman, A. L. Atkinson, G. C. Schatz, *Acc. Chem. Res.* **2008**, *41*, 1710.
[15] C. Catala, B. Mir-Simon, X. Feng, C. Cardozo, N. Pazos-Perez, E. Pazos, S. Gómez-De Pedro, L. Guerrini, A. Soriano, J. Vila, F. Marco, E. Garcia-Rico, R. A. Alvarez-Puebla, *Adv. Mater. Technol.* **2016**, *1*, 1600163.
[16] B. Mir-Simon, I. Reche-Perez, L. Guerrini, N. Pazos-Perez, R. A. Alvarez-Puebla, *Chem. Mater.* **2015**, *27*, 950.
[17] R. Holze, *Phys. Chem. Chem. Phys.* **2015**, *17*, 21364.
[18] A. M. Schwartzberg, C. D. Grant, A. Wolcott, C. E. Talley, T. R. Huser, R. Bogomolni, J. Z. Zhang, *J. Phys. Chem. B* **2004**, *108*, 19191.
[19] N. S. Mueller, E. Pfitzner, Y. Okamura, G. Gordeev, P. Kusch, H. Lange, J. Heberle, F. Schulz, S. Reich, *ACS Nano* **2021**, *15*, 5523.
[20] H. J. Singh, D. Misatziou, C. Wheeler, A. Buendía, V. Giannini, J. A. Sánchez-Gil, M. H. V. Werts, T. Brown, A. H. El-Sagheer, A. G. Kanaras, O. L. Muskens, *ACS Appl. Opt. Mater.* **2023**, *1*, 69.
[21] M. Blanco-Formoso, N. Pazos-Perez, R. A. Alvarez-Puebla, *ACS Omega* **2020**, *5*, 25485.